The Probabilistic Robot Kinematics Model and its Application to Sensor Fusion

Lukas Meyer[1], Klaus H. Strobl[1], and Rudolph Triebel[1]

***Abstract*— Robots with elasticity in structural components can suffer from undesired end-effector positioning imprecision, which exceeds the accuracy requirements for successful manipulation. We present the Probabilistic-Product-Of-Exponentials robot model, a novel approach for kinematic modeling of robots. It does not only consider the robot's deterministic geometry but additionally models time-varying and configuration-dependent errors in a probabilistic way. Our robot model allows to propagate the errors along the kinematic chain and to compute their influence on the end-effector pose. We apply this model in the context of sensor fusion for manipulator pose correction for two different robotic systems. The results of a simulation study, as well as of an experiment, demonstrate that probabilistic configuration-dependent error modeling of the robot kinematics is crucial in improving pose estimation results.**

I. Introduction

Robots require sufficient accuracy to manipulate objects. The accuracy is defined by the application and can range from centimeters to submilimeters. Classic industrial manipulators usually fulfill the accuracy requirements and their positioning is commonly assumed to be exact during the manipulation process.

However, robots with elastic components are becoming common in research but can suffer from undesired positioning imprecision that exceeds the accuracy requirements imposed by the application. The elasticity can be introduced to the system on purpose to allow for intrinsically compliant robots or can be a side effect of additional design constraints. One example is the DLR Lightweight Rover Unit (LRU, shown in Fig. 1), where lightweight materials cause structural bending during the manipulation process. Another example is the emerging low-budget robotic arms that trade accuracy for simplicity.

Kinematic errors of robots have traditionally been mitigated by calibration procedures prior to starting the actual robot operations, namely the manipulator calibration and the camera-to-robot calibration. Using static calibration alone, however, imposes constraints on the robot model, such as that the error parameters are constant and that there are enough sensors to fully observe all degrees of freedom (DoF) of the robot. This assumption is violated once we consider time-varying, configuration-dependent errors or unobservable parts of the forward kinematics. Instead, online error correction strategies must be employed (e. g., camera observation of the manipulator or the use of tracking devices).

[1]All authors are with the Institute of Robotics and Mechatronics, German Aerospace Center (DLR), 82234 Wessling, Germany firstname.lastname@dlr.de

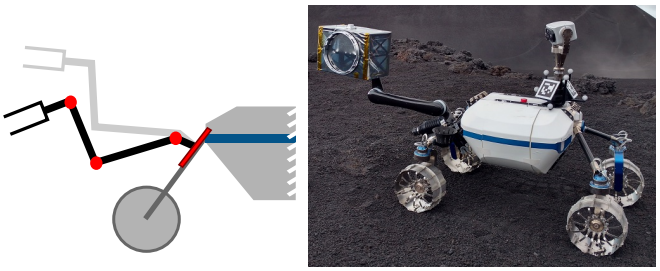

Fig. 1: The Lightweight Rover Unit (LRU) [1]: During manipulation, structural elasticities (red) cause undesired, configuration-dependent positioning offsets in the real robot (black) compared to the nominal forward kinematics (gray). Image: © DLR.

Such online techniques require an adequate probabilistic kinematic model of the robot that allows to represent varying kinematic errors and provides the means to propagate the error from its source along the kinematic chain. The error propagation is of special relevance, as small rotational errors in the kinematic chain are not directly observable but can result in significant displacements at the robot's end-effector. In this paper, we formulate the robot forward kinematics in a way such that they encode the error correlations of the kinematic chain and that they can be used as an independent sensor input for online correction strategies.

We propose the use of the *Probabilistic Product-Of-Exponentials* robot model (PPOE) that augments the *local Product-Of-Exponentials* (POE) robot model of [2] by a probabilistic representation of kinematic errors. We consider all relative transformations *and perturbations* in the kinematics as elements of a Lie group, the Special Euclidean group $SE(3)$. This allows us to use a wide set of mathematical tools to propagate and compose all perturbations along the forward kinematics towards the end-effector or any other desired frame of reference. Our general Lie group-based formulation additionally allows for straightforward adaptation of the perturbation model to another Lie group-based robot representations, e. g., the piecewise constant curvature model for continuum robots [3].

We propose the PPOE model in combination with sensor fusion for manipulator pose correction as the principal application in mind. The idea is that improved knowledge on the robot kinematics leads to an improved estimate of the 6DoF pose of the end-effector.

We argue that despite being erroneous, the forward kinematics is still rich in information. The kinematics can effectively be considered as a high-frequency, low-computational-cost principal sensor for manipulator pose estimation al-

gorithms. Relying on the forward kinematics as principal sensor loosens the requirements for the other sensors, e. g., in frequency or dimensions.

In this work, we show sensor fusion scenarios with two of our robotic systems: a) a simulation study of object contact interaction by a humanoid robot and b) experiments of manipulator pose correction using the principal camera on our planetary rover prototype LRU (Fig. 1). Both scenarios have in common that we do not measure the full manipulator pose with the additional sensors but use lower dimensional measurements instead. The idea is that sensors that measure only a subset of the full robot pose can be fused with the PPOE kinematics to allow for significant pose improvements.

The contributions of the paper are as follows:

- We present the PPOE model, a probabilistic formulation of the robotic forward kinematics in Section IV and provide an illustrative example.
- We discuss the advantages of the PPOE model and list the limitations.
- We showcase the potential of the PPOE kinematics modeling in two proof-of-concept applications with a pose fusion scheme based on a Lie group Extended Kalman Filter architecture (Section V). The first application illustrates in a simulation how a correct correlation representation of the error allows for a better pose estimate. The importance of considering the dependence of the kinematic error with respect to (w.r.t) the change of robot configuration is shown in the second application as experiment.

II. Related work

Our work combines the aspects of error and uncertainty propagation in $SE(3)$ with the field of robot kinematic modeling.

Regarding uncertainty representation for poses, we mostly follow [4] who consider the Lie group character of poses to represent, propagate, and manipulate uncertainties. Contrary to their approach, we formulate our model w.r.t. local reference frames.

Early work on this topic includes [5], who already consider first-order uncertainty propagation on Lie groups and use it to model spatial relationships in the workspace during robotic manipulation. The work of [4] is closely related to the works of [6] and [7] and differ in the specific definition of perturbation; a detailed discussion of the differences is provided by [4] itself. A major field of application of Lie group-based uncertainty representation is robot navigation, i. e. state estimation and SLAM [8].

Wang and Chirikjian [9] apply error propagation and uncertainty representation specifically to manipulator kinematics in order to model the influence that errors in the robot's structure have on the pose of the end-effector. However, they limit their approach to specific applications and do not consider a generalized robot model for arbitrary error sources.

Regarding the robot kinematic modeling, many different conventions exist. A well-known generalized approach is the Denavit-Hartenberg convention and its multiple adaptations (see [10, p. 23f]). In our case, however, we require a convention that is based on the concept of Lie groups, such that we can more naturally incorporate the handling of uncertainties using the methods of the previously mentioned works. The POE convention (see [11, p. 82f]) is such a representation. More specifically, we build our work on the *local POE* as introduced by [2] and augment it with the uncertainty representation of [4]. To the best of our knowledge, no other works exist in the literature that combine a generalized robot kinematics convention with uncertainty representations.

Our primary intended use case for the PPOE model is in sensor fusion with low-frequency and low-dimensional sensors for robot pose estimation. The work of [12] uses high frequency depth images for 6D manipulator pose estimation, but only use the kinematic information for initialization. The algorithm from [13] uses similar sensor information in a particle filter based architecture. Even though it corrects for errors in the joint measurements and camera-to-base transformation, a further generalization of error sources is omitted. Regarding deep learning-based approaches, amongst others, [14] detect key-points on robotic manipulators but assume the kinematics within the robot to be exact and only apply a camera-to-robot-base pose correction.

III. Mathematical Background

We consider robotic manipulators that can be modeled with a tree structure of interconnected individual rigid bodies, namely links connected by joints. The relation between the elements of the robot are described using poses. A pose $\mathcal{X}$ is the composition of rotation and translation of a rigid body and can be represented as element of the *special Euclidean group* $SE(3)$ [11, p. 35], i. e. using homogeneous transformation matrices

$$\mathcal{X} = \begin{bmatrix} \boldsymbol{R} & \boldsymbol{t} \\ \boldsymbol{0} & 1 \end{bmatrix}, \qquad \boldsymbol{t} \in \mathbb{R}^3, \boldsymbol{R} \in SO(3) \tag{1}$$

containing the rotation matrix $\boldsymbol{R}$ as element of the special orthogonal group $SO(3)$ and the translation vector $\boldsymbol{t}$. The origin frame of $SE(3)$ is denoted as $\mathcal{E}$, the identity matrix.

The $SE(3)$ is a *Lie group* which allows the application of a wide set of mathematical tools. An excellent and concise overview regarding Lie groups can be found in [15], whose notation we mostly follow.

We briefly present the notations and operators used in this work. A pose $\mathcal{X}$ evolves on a manifold $\mathcal{M}$ (in our case $SE(3)$) that is defined by the Lie group's properties - see [15] for details. Around any $\mathcal{X}$ on that manifold, locally linear coordinates ${}^{\mathcal{X}}\boldsymbol{\xi}^{\wedge}$ (also called the *Lie algebra* $\mathfrak{se}(\mathbf{3})$) can be established that 'live' in the corresponding *tangent space* $\mathcal{TM}_{\mathcal{X}}$.

The $\wedge$-decorator illustrates that ${}^{\mathcal{X}}\boldsymbol{\xi}^{\wedge}$ is an element of the tangent space, however any element can also be expressed as cartesian vector $\boldsymbol{\xi}$ with

$$\boldsymbol{\xi}^{\wedge} = \begin{bmatrix} [\boldsymbol{\theta}]_{\times} & \boldsymbol{\rho} \\ \boldsymbol{0} & 0 \end{bmatrix} \in \mathfrak{se}(\mathbf{3}), \quad \boldsymbol{\xi} = \begin{bmatrix} \boldsymbol{\rho} \\ \boldsymbol{\theta} \end{bmatrix} \in \mathbb{R}^6, \tag{2}$$

where $[\ ]_{\times}$ denotes a skew-symmetric matrix, and $\boldsymbol{\rho}, \boldsymbol{\theta} \in$

$\mathbb{R}^3$ denote the translational and rotational components in the tangent space.

The *exponential map* allows to map $\boldsymbol{\xi}^\wedge$ into elements of $SE(3)$ and the *logarithmic map* reverses the operation [15]:

$$\exp : \mathcal{TM}_\mathcal{X} \to \mathcal{M}; \quad \boldsymbol{\xi}^\wedge \mapsto \mathcal{X} = \exp(\boldsymbol{\xi}^\wedge), \tag{3}$$

$$\log : \mathcal{M} \to \mathcal{TM}_\mathcal{X}; \quad \mathcal{X} \mapsto \boldsymbol{\xi}^\wedge = \log(\mathcal{X}). \tag{4}$$

Note that the capitalized exponential and logarithmic maps allow us to omit the intermediate step of Lie Algebra representation and to directly work with vectors $\boldsymbol{\xi}$ instead, with $\mathcal{X} = \operatorname{Exp}(\boldsymbol{\xi})$ and $\boldsymbol{\xi} = \operatorname{Log}(\mathcal{X})$ respectively.

A. Incrementing in $SE(3)$

Consider a pose $\mathcal{Y}$ that is the result of incrementing $\mathcal{X}$ by a $\boldsymbol{\xi}$. The increment can either be expressed globally w.r.t. the origin $\mathcal{E}$ or locally w.r.t. $\mathcal{X}$. Then, the following identity holds [15]:

$$\mathcal{Y} = \operatorname{Exp}({}^\mathcal{E}\boldsymbol{\xi})\mathcal{X} = \mathcal{X}\operatorname{Exp}({}^\mathcal{X}\boldsymbol{\xi}), \tag{5}$$

which means that $\mathcal{X}$ can be incremented either globally around its origin using ${}^\mathcal{E}\boldsymbol{\xi}$ or locally at $\mathcal{X}$ using ${}^\mathcal{X}\boldsymbol{\xi}$, yielding the same result. However, due to the non-commutativity of $SE(3)$, ${}^\mathcal{E}\boldsymbol{\xi}$ and ${}^\mathcal{X}\boldsymbol{\xi}$ are not the same but comply to the following identity

$${}^\mathcal{E}\boldsymbol{\xi} = \mathbf{Ad}_\mathcal{X}\, {}^\mathcal{X}\boldsymbol{\xi}, \tag{6}$$

that uses the *adjoint matrix* $\mathbf{Ad}$ w.r.t. $\mathcal{X}$ to linearly map the tangent vectors $\boldsymbol{\xi}$ between different points on a manifold [15].

The adjoint matrix is calculated as

$$\mathbf{Ad} = \begin{bmatrix} \boldsymbol{R} & [\boldsymbol{t}]_\times \boldsymbol{R} \\ \mathbf{0} & \boldsymbol{R} \end{bmatrix} \in \mathbb{R}^{6\times 6}. \tag{7}$$

Equation (6) illustrates that the rotational part of an increment stays constant in magnitude anywhere on the manifold, but additionally contributes to the translational part scaled by $\boldsymbol{t}$. This is of key relevance for the error propagation presented in Section IV, as it shows that small rotational changes can cause significant translational offsets further away, but the influence of translational changes remains constant everywhere.

B. Uncertainties in $SE(3)$

We express uncertainties of poses as covariances in their respective tangent space [6, p. 376], using the proposed framework of [4]. Consider a pose $\mathcal{X}$ that is locally perturbed around its mean value $\bar{\mathcal{X}}$ by a $\boldsymbol{\xi} \in \mathcal{TM}_\mathcal{X}$, thus

$$\mathcal{X} = \bar{\mathcal{X}} \operatorname{Exp}({}^\mathcal{X}\boldsymbol{\xi}). \tag{8}$$

Note that we apply the perturbation around the point $\bar{\mathcal{X}}$ that results in a *right multiplicative*, local representation of perturbations (following [15]), contrary to the global, *left multiplicative* representation used by [4].

The corresponding covariance matrix $\boldsymbol{\Sigma}_\mathcal{X} \in \mathbb{R}^{6\times 6}$ is [15]

$$\boldsymbol{\Sigma}_\mathcal{X} := \mathbb{E}[\boldsymbol{\xi}\boldsymbol{\xi}^T] = \mathbb{E}[\operatorname{Log}(\bar{\mathcal{X}}^{-1}\mathcal{X})\operatorname{Log}(\bar{\mathcal{X}}^{-1}\mathcal{X})^T], \tag{9}$$

and can be mapped to other tangent spaces using the adjoint matrix (e. g., expressed globally at the origin [15])

$$\boldsymbol{\Sigma}_\mathcal{E} = \mathbf{Ad}_\mathcal{X} \boldsymbol{\Sigma}_\mathcal{X} \mathbf{Ad}_\mathcal{X}^T. \tag{10}$$

C. Composition of uncertain poses

To describe the forward kinematics, it is necessary to compound several poses and their corresponding covariance matrices. The approach by [4] (rewritten as right multiplicative) is summarized in the following. Consider two relative poses that are each perturbed with a zero-mean, normal distributed $\boldsymbol{\xi}_i$, and are fully described by the mean pose and an associated covariance matrix $[\bar{\mathcal{X}}_i, \boldsymbol{\Sigma}_{\mathcal{X}_i}]$, with $i = 1, 2$. The compounded pose $\mathcal{X}_{12}$ with $[\bar{\mathcal{X}}_{12}, \boldsymbol{\Sigma}_{\mathcal{X}_{12}}]$ is therefore

$$\mathcal{X}_{12} = \bar{\mathcal{X}}_1 \operatorname{Exp}(\boldsymbol{\xi}_1)\bar{\mathcal{X}}_2 \operatorname{Exp}(\boldsymbol{\xi}_2), \tag{11a}$$

$$= \bar{\mathcal{X}}_1\bar{\mathcal{X}}_2 \operatorname{Exp}(\mathbf{Ad}_{\mathcal{X}_2^{-1}}\boldsymbol{\xi}_1) \operatorname{Exp}(\boldsymbol{\xi}_2), \tag{11b}$$

$$= \bar{\mathcal{X}}_1\bar{\mathcal{X}}_2 \operatorname{Exp}(\boldsymbol{\xi}_1') \operatorname{Exp}(\boldsymbol{\xi}_2), \tag{11c}$$

$$= \bar{\mathcal{X}}_{12} \operatorname{Exp}(\boldsymbol{\xi}_{12}). \tag{11d}$$

Note that the zero-mean assumption for the perturbations needs to hold for step (11b).

In (11d), both individual perturbations are compounded, which is calculated using the *Baker–Campbell–Hausdorff formula* (BCH) [4]. It takes into account that all $\boldsymbol{\xi}_i$ cannot be added together directly, as they are still in slightly different reference frames. Using BCH provides an infinite series [4]

$$\begin{aligned}\boldsymbol{\xi}_{12} = \boldsymbol{\xi}_1' + \boldsymbol{\xi}_2 + \frac{1}{2}\boldsymbol{\xi}_1'^\curlywedge\boldsymbol{\xi}_2 + \frac{1}{12}\boldsymbol{\xi}_1'^\curlywedge\boldsymbol{\xi}_1'^\curlywedge\boldsymbol{\xi}_2 \\ + \frac{1}{12}\boldsymbol{\xi}_2^\curlywedge\boldsymbol{\xi}_2^\curlywedge\boldsymbol{\xi}_1' - \frac{1}{24}\boldsymbol{\xi}_2^\curlywedge\boldsymbol{\xi}_1'^\curlywedge\boldsymbol{\xi}_1'^\curlywedge\boldsymbol{\xi}_2 + \cdots,\end{aligned} \tag{12}$$

with

$$\boldsymbol{\xi}^\curlywedge = \begin{bmatrix} [\boldsymbol{\theta}]_\times & [\boldsymbol{\rho}]_\times \\ \mathbf{0} & [\boldsymbol{\theta}]_\times \end{bmatrix}. \tag{13}$$

This series is inserted in the covariance definition (9), yielding

$$\mathbb{E}[\boldsymbol{\xi}_{12}{\boldsymbol{\xi}_{12}}^T] = \mathbb{E}\Big[\boldsymbol{\xi}_1'\boldsymbol{\xi}_1'^T + \boldsymbol{\xi}_2\boldsymbol{\xi}_2^T + \cdots\Big] \tag{14}$$

and can be evaluated up to the desired order of accuracy. For the applications in this work, we evaluate the series for the first two terms, yielding

$$\begin{aligned}\boldsymbol{\Sigma}_{12} &= \mathbb{E}\big[\boldsymbol{\xi}_1'\boldsymbol{\xi}_1'^T\big] + \mathbb{E}\big[\boldsymbol{\xi}_2\boldsymbol{\xi}_2^T\big], \\ &= \mathbf{Ad}_{\mathcal{X}_2^{-1}}\boldsymbol{\Sigma}_1\mathbf{Ad}_{\mathcal{X}_2^{-1}}^T + \boldsymbol{\Sigma}_2.\end{aligned} \tag{15}$$

There is an ambiguity in the literature: our approximation is referred to as second order [4] or first order [7] respectively. For approximations of next-higher order the nomenclature is consequently fourth or second order, respectively.

We plan to include higher order approximations of (14) in future work, as the approximation error becomes relevant especially for high perturbation values [4].

IV. Probabilistic Product-Of-Exponentials Robot Model

We present a robot kinematic convention that allows a straightforward incorporation of the perturbation modeling introduced in Section III. We modify the *local POE* [2] and augment it with probabilistic terms considering generic concentrated perturbation sources in a manipulator.

We refer to the result as *Probabilistic Product-Of-Exponentials* robot kinematic model, as it encodes both

geometry and probabilistic perturbations as tangent space elements and combines these using the exponential map.

A. Model

A robotic manipulator consists of links and joints, where an assembly of two links i and $i+1$ is connected by a joint. Analogous to [2], we split the kinematic description into several relative poses and consider link i and its corresponding joint combined w.r.t. a local reference frame $\mathcal{F}_i$, as shown in Fig. 2. The relative pose between $\mathcal{F}_i$ and $\mathcal{F}_{i+1}$ is

$$\mathcal{X}_{i,i+1}(q_i) = \operatorname{Exp}(\boldsymbol{p}_i)\operatorname{Exp}(\boldsymbol{\xi}_i)\operatorname{Exp}(\boldsymbol{\zeta}_i q_i), \tag{16}$$

where

- $\boldsymbol{p}$ denotes the static transformation w.r.t. the nominal link geometry, depicted as intermediate frame $\mathcal{F}_{i,p}$ (green) in Fig. 2.
- $\boldsymbol{\xi}$ is a perturbation in the robot kinematics, describing the offset between the nominal and real joint axes. It is shown in Fig. 2 as $\mathcal{F}_{i,\xi}$ (gray).
- $\boldsymbol{\zeta}$ defines the direction of a joint movement with an amplitude of q, thus in combination denote the time-varying joint movement around the joint axis, resulting in $\mathcal{F}_{i+1}$. Note that the unit-vector $\boldsymbol{\zeta}$ can be used to represent both prismatic and revolute joints [11, p. 85], with all entries except one set to zero.

In our approach, the perturbation is located behind the static transformation. This representation allows to correct the true axis of rotation for the subsequent joint, see [16, p. 194f]. Obviously, the presented order of transformations can be modified to suite other specific kinematic problems.

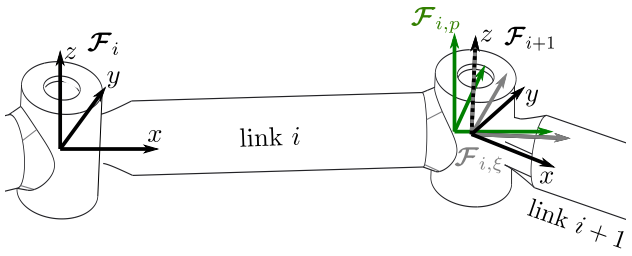

Fig. 2: Frames of the PPOE model for a link i: $\mathcal{F}_{i,p}$ (green) denotes the nominal rigid link geometry. $\mathcal{F}_{i,\xi}$ (gray) is the correct (true) rigid link geometry. $\mathcal{F}_{i+1}$ denotes the joint frame after a movement of q_i around the joint rotation axis (it coincides with an axis of $\mathcal{F}_{i,\xi}$ - here around the z-axis).

For the manipulator, the full kinematic chain is expressed as

$$\mathcal{X}_{0,n+1} = \Big(\prod_{i=1}^{n} \mathcal{X}_{i,i+1}(q_i)\Big)\operatorname{Exp}(\boldsymbol{p}_{n+1}), \tag{17}$$

where n denotes the number of joints and $\operatorname{Exp}(\boldsymbol{p}_{n+1})$ is the relative pose of the end-effector w.r.t. the last joint. Kinematics in a tree-structure (e. g., dual manipulators) can be modeled as individual chains for each branch.

B. Kinematics computation

The probabilistic forward kinematics from the PPOE model are the mean pose together with the corresponding covariance matrix of the end-effector (or any other desired frame along the chain), thus forming $[\bar{\mathcal{X}}_{0,n+1}, \boldsymbol{\Sigma}_{\mathcal{X}_{0,n+1}}]$. To obtain the mean pose $\bar{\mathcal{X}}_{0,n+1}$, we evaluate (17) with all $\boldsymbol{\xi}_i = \mathbf{0}$.

The corresponding covariance $\boldsymbol{\Sigma}_{\mathcal{X}_{0,n+1}}$ is obtained by compounding the individual covariances sequentially along the kinematic chain, using (14) up to the desired order. For example, with our approximation in (15), the covariance matrix at the location of perturbation i is

$$\boldsymbol{\Sigma}_{\mathcal{X}_{0,i}} = \mathbf{Ad}_{\mathcal{X}_{i,i-1}} \boldsymbol{\Sigma}_{0,i-1} \mathbf{Ad}^T_{\mathcal{X}_{i,i-1}} + \boldsymbol{\Sigma}_i, \tag{18}$$

where $\boldsymbol{\Sigma}_{0,i-1}$ is the composition of all previous covariances.

This is a key aspect of the PPOE model: it encodes in the resulting covariance matrix how errors in each of the six dimensions of the end-effector pose correlate with each other, given perturbations that do not originate at the end-effector itself but instead within the robot's kinematic chain.

C. Example

We illustrate the concept of the PPOE model on an exemplary planar robot arm with three revolute joints, as shown in Fig. 3. The perturbations are marked in red and are – to simplify this example – only of rotational character around the joint axes. The resulting uncertainty regarding the end-effector pose is calculated using the PPOE model, where the 80% confidence interval is plotted in blue for the translational component. Furthermore, we provide Monte-Carlo samples of the end-effector poses (green dots) as comparison.

In Fig. 3a, only a perturbation on the first joint axis is considered, thus resulting in a probability distribution at the end-effector that resembles a circular arc. This is exactly what to expect, considering the perturbation propagation described by (6), i. e. the rotational error at the joint causes a significant displacement at the end-effector.

The other examples consider equal-valued perturbations on all joint-axes. This introduces a widening of the arc, resulting in the well-known *banana-distribution* [17] in Fig. 3b. Note that the pose in Fig. 3b is a singular configuration of the robot thus all individual perturbations result in translational errors at the end-effector with the identical direction. In cases where the perturbations combine with a higher angle w.r.t. each other, the covariance is bulged towards a more elliptical shape (Figs. 3c and 3d)

In general, this way of representing the pose uncertainty is correct but conservative as the comparison with the sampled poses shows. Nevertheless, it is a much more accurate representation than classical approaches such as ellipses. See [4] for an analysis on approximation errors. Figure 3 underlines the fact that end-effector errors and the corresponding covariance matrix are highly configuration dependent, which has to be considered for applications.

For visualizing the covariances, we follow the same approach as [4] in their example: The covariance matrix is scaled to the desired confidence interval and its eigenvalues and -vectors are computed. For all pairwise eigenvector combinations, six-dimensional ellipsoids are computed in the tangent space $\mathcal{TM}_{\mathcal{X}}$. The resulting representation for $\mathcal{X}$ is

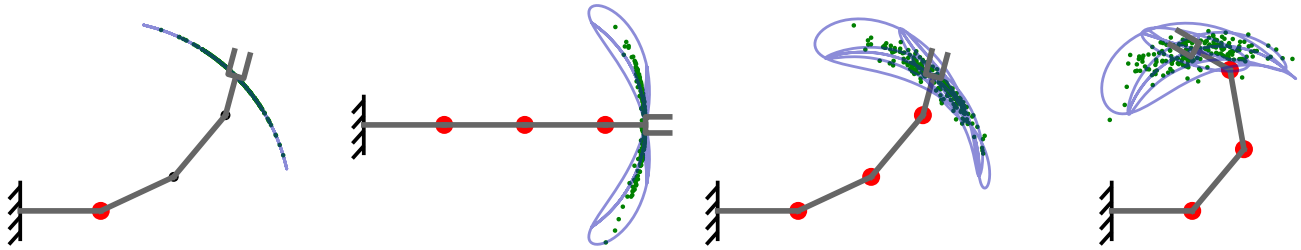

(a) (b) (c) (d)

Fig. 3: Example of the PPOE model with a 3DoF planar manipulator. The robot joints are marked with circles, with pure angular perturbations of 10° standard deviation (red). The 80% enclosure of the covariance is shown in blue. As comparison, a sampling of the end-effector pose is given (green, 200 samples each). (a) shows the uncertainty distribution for a perturbation in the first joint, resulting in a one-dimensional position error. (b) shows the banana shape for three compounded perturbations, where all perturbations have the same principal direction of influence on the end-effector due to a singular robot configuration. In (c), the perturbations act on the end-effector pose with non-parallel principal directions, causing a widening of the banana. (d) shows how the banana shape becomes more elliptical, once the angles between the principal directions increase further due to the change in robot configuration.

obtained by converting all elements on the ellipsoid surface into elements of the manifold $\mathcal{M}$ using the exponential map. As final step, all elements are transformed into the global frame $\mathcal{E}$ and are visualized. The underlying probability distribution is Gaussian only in the tangent space $\mathcal{TM}_\mathcal{X}$, and the transformation onto the manifold creates the shapes seen in Fig. 3.

D. Simplifications and Discussion

The PPOE model contains two key simplifications w.r.t. the error modeling. First, it only considers concentrated error sources within the kinematic chain and therefore does not allow to directly model e. g., continuous deflections like in continuum material robots. This simplification can be considered valid, as (6) shows that rotational and translational errors propagate constant individually. Furthermore, for the rotational influence on the translation error, only the correct lever needs to be assigned to the rotation error location. Thus, continuum errors can be concentrated onto discrete locations.

Second, the PPOE model considers zero-mean probabilistic errors and uses a probability distribution that is Gaussian in the tangent space. Any non-zero-mean offset can therefore not be modeled directly. However, it still correctly captures the principal directions of error influence at any frame of reference. For sensor fusion schemes, we therefore argue that the resulting covariance matrix of PPOE is a valuable tool to consistently weight the forward kinematics information in combination with other observations of the robot pose.

Optionally, restricting perturbations in several DoF in the PPOE model can be an application-oriented simplification. We argue that in many cases, rotational errors can be considered the dominant error source as they get scaled by the respective distance to the target frame. Subsequently, translational error sources can be neglected for such scenarios. Furthermore, if knowledge of the system exists regarding its principal error sources, all other errors can be restricted to zero if assumed to be negligible.

The general formulation of PPOE allows for arbitrary customization. As example, the user can simply set all $\boldsymbol{\xi} = \boldsymbol{\zeta}$ and assign variances to these perturbations in the desired magnitude to explicitly model errors in the joint angles. If the PPOE model is to be applied to other kinematic modeling approaches, such as the piecewise constant curvature kinematics [3] for continuum soft robots, their exponential coordinate model can be augmented by perturbations in identical manner to (16) and the same mathematical tools can be applied.

Additionally, the forward kinematics can be extended to model uncertainties in grasp linkage. For this, a new end-effector frame is defined by the grasped object which is described probabilistically by adding $\boldsymbol{p}_{\text{grasp}}$ and $\boldsymbol{\xi}_{\text{grasp}}$ to (17).

A POE kinematic description for parallel manipulators is discussed in [11, p. 133]. PPOE can potentially be used there as well, e. g., using the fused end-effector pose of all parallel branches as reference in the *structure equation*. However, detailing this remains for future research.

V. Application: Probabilistic Kinematics in Sensor Fusion

We devised the PPOE model with the application to sensor fusion in mind. The covariance matrix of the end-effector pose defines how additional (low-dimensional) sensor measurements are weighted in the fusion process. The idea is that using a covariance matrix which is consistent with the real errors of the system improves the accuracy of the fused pose. We investigate how a weighting of measurements guided by the PPOE covariance influences the fusion result, compared to a 'naive' approach using static and uncorrelated covariance matrices.

We illustrate this proof-of-concept with two different sensor fusion examples. The first application is a simulation study of a humanoid robot that can sense contact with other objects of known but uncertain poses as illustrated in Fig. 4. It is used to showcase the importance of correlation in the covariance matrix.

The second example shows pose correction for the LRU's end-effector (Fig. 1), where camera observations are combined with the forward kinematics. Here, we show how the configuration dependency of the error influences the estimation results.

A. Lie group-EKF Framework

The state is the pose $\mathcal{X}$ of the end-effector. To correct $\mathcal{X}$, we use the update step of an extended Kalman filter (EKF) that considers the underlying Lie group structure of the problem, thus named LG-EKF [18].

Note, that we only consider the update process of a static state regarding single measurements to illustrate the usability of the PPOE model. Discussion and implementation of an applicable online fusion architecture of the LG-EKF exceeds the scope of this letter and is left for future work.

We initialize the state $\mathcal{X}_0$ as the mean end-effector pose obtained from the kinematics together with the associated covariance matrix $\mathbf{\Sigma}_{\mathcal{X},0}$. The sensor measurement is

$$\boldsymbol{z} = h(\mathcal{X}, \boldsymbol{v}), \tag{19}$$

where $\boldsymbol{v} \sim \mathcal{N}(\mathbf{0}, \mathbf{\Sigma}_v)$ is the zero mean measurement noise characterized by its covariance matrix $\mathbf{\Sigma}_v$.

We can therefore correct the initial pose by the following measurement step (adapted from [18]) to

$$\boldsymbol{K}_k = \mathbf{\Sigma}_{\mathcal{X},k} \boldsymbol{H}_k^T (\boldsymbol{H}_k \mathbf{\Sigma}_{\mathcal{X},k} \boldsymbol{H}_k^T + \mathbf{\Sigma}_v), \tag{20}$$

$$\boldsymbol{m}_k = \boldsymbol{K}_k (\boldsymbol{z}_k - h(\mathcal{X}_k, \mathbf{0})), \tag{21}$$

$$\mathcal{X}_{k+1} = \mathcal{X}_k \operatorname{Exp}(\boldsymbol{m}_k), \tag{22}$$

$$\mathbf{\Sigma}_{\mathcal{X},k+1} = (\boldsymbol{I} - \boldsymbol{K}_k \boldsymbol{H}_k) \mathbf{\Sigma}_{\mathcal{X},k}. \tag{23}$$

The state correction $\boldsymbol{m} \in \mathbb{R}^6$ is expressed in the tangent space of the state. The update is applied iteratively, denoted with k. $\boldsymbol{K}$ represents the *Kalman gain* and $\boldsymbol{H}$ and $\boldsymbol{M}$ are the linearization Jacobians of (19)

$$\boldsymbol{H}_k = \left.\frac{\partial h_k}{\partial \mathcal{X}}\right|_{\mathcal{X}_k}, \qquad \boldsymbol{M}_k = \left.\frac{\partial h_k}{\partial \boldsymbol{v}}\right|_{\mathcal{X}_k}. \tag{24}$$

These Jacobians can be computed numerically following [19] by applying variations to the tangent space around the state and on the noise.

B. Simulation Study: Pose Correction by Contact Sensing

The DLR humanoid robot David (Fig. 4), has three principal sources of kinematic errors: First, David has a continuum-elastic neck, where several sophisticated pose estimation algorithms yield accuracies of $0.5°$ to $5°$ for the transformation between head and torso [20]. Second, the wrist kinematics are nonlinear [21], therefore a modeling as two revolute joints causes approximation errors. Last, we consider inaccurate measurements in the finger joints.

The simulation setup is illustrated in Fig. 4. David uses its stretched index finger to touch a table in front of it. Integrating contact sensors at the fingertips of the physical David robot is work in progress. We therefore consider a detected table interaction as a simulated one-dimensional measurement source to our estimation algorithm.

The table surface is modeled as a pose with covariance matrix $\mathbf{\Sigma}_v = \operatorname{diag}(0.5, 0.5, 0.001, 0.017, 0.017, 0.17)$ that

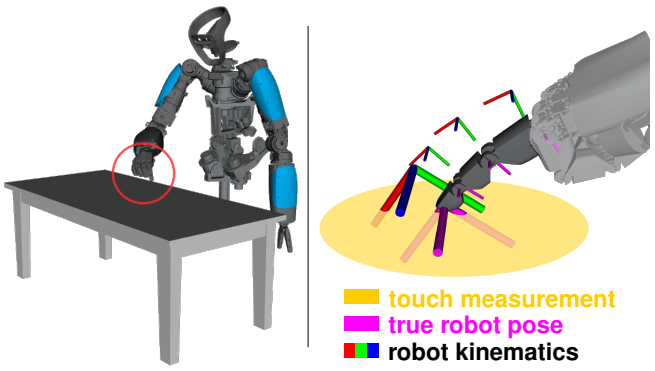

Fig. 4: The DLR humanoid *David* interacts with a table surface in the simulation study. The contact between its index finger and the table surface is the noisy 1D measurement (orange) to correct the erroneous kinematics (frames visualized in RGB-colors) to match the true kinematic frames (purple).

symbolizes a small error in the direction and the orientation of the surface's normal vector and a high error otherwise. It can be imagined as a measurement, where the table plane is recognized by a depth camera. The measurement error in (21) is the distance between the predicted fingertip position and the table surface along the surface's normal direction during contact. The measurement information is then transformed from the reference frame of the table into the reference frame of the end-effector. The kinematic errors described before are all set to a static offset with values between one and two degrees, to simulate erroneous forward kinematics.

Once David establishes contact with the table, the forward kinematics from the PPOE model are iteratively corrected by the algorithm of Section V-A. The results are shown as solid lines in Fig. 5. It can be seen that the positional error in Fig. 5a converges to a small residual for all degrees of freedom and the resulting covariance matrix of the state decreases in its eigenvalues, indicating an increase in confidence w.r.t. the pose (Fig. 5c).

We stated before that one of the main goals of the PPOE model is to encode the correlation between kinematic errors and to describe their influence onto the end-effector pose, which is done by the covariance matrix. Indeed, if we would use a naive approach and model all end-effector errors as independent (this is essentially dropping all non-diagonal entries of the covariance matrix), we are only able to correct the pose in the observable direction and the residual error stays relatively high, see dashed lines in Fig. 5a.

The rotation error (Fig. 5b) is not significantly corrected in either setup, however an error of two degrees at the end-effector itself can usually be considered sufficiently small for successful manipulation.

C. Experiment: 2D camera measurements for manipulator pose correction

We motivated our work using the planetary rover prototype LRU (Fig. 1) as an example. It is equipped with a Jaco2 arm from Kinova that is mounted on a carbon-fiber plate at the rear of the rover. For our experiment, we correct the end-effector pose of the LRU by observing fiducial markers

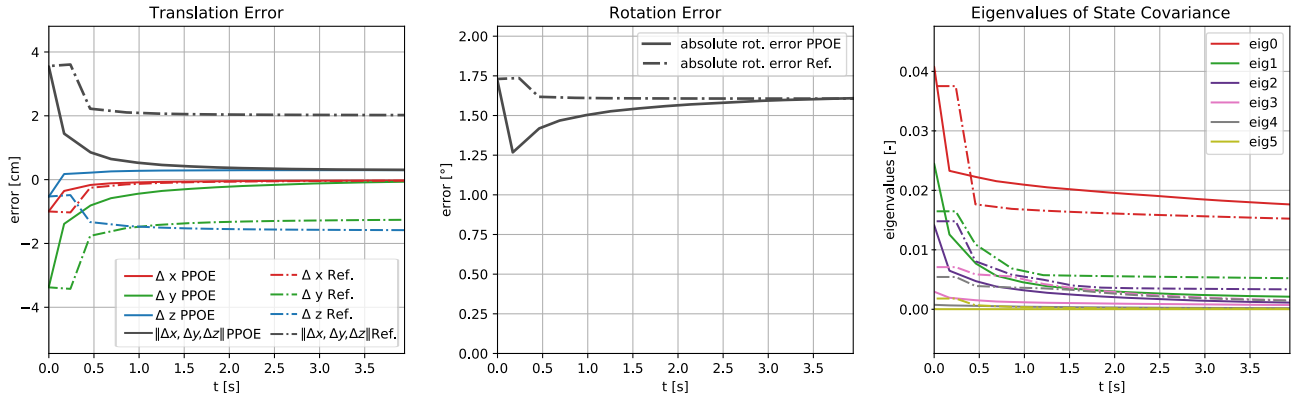

(a) (b) (c)

Fig. 5: Residual pose errors of the end-effector, i. e. the finger-tip of David's index finger, during the contact phase with a simulated table surface. The residual error of the pose estimation is shown for two cases, using the covariance matrix computed by the PPOE model (solid lines) and for a covariance matrix that naively assumes independence of the state variables (dashed lines). PPOE enables us to encode a strong correlation between the positional state variables and therefore allows for a better pose estimate w.r.t. translational components (a). The absolute rotational error is mostly unaffected by either approach (b). The decreasing eigenvalues of the covariance matrix during the contact phase illustrate an increase in confidence w.r.t. the true manipulator pose (c).

(AprilTags [22]) on the end-effector and fuse their 2D bearings information with the 6D pose from the kinematics. We model the forward kinematics of the LRU using the PPOE model and assign errors using our knowledge of the system. The most prominent error source is the base plate where the manipulator is mounted, as it bends under load. We assign an error with standard deviation of 1° and 5° in horizontal and vertical directions, respectively. Along the joints, we assign errors with 0.5° standard deviation. These are conservative heuristic estimates to account for changes in load and for potential de-calibration. The magnitude is motivated by the fact that the hand-eye-calibration [23] results in a residual error of 2.1° and $1.9\,\text{cm}$ at the end-effector.

Equation (19) becomes

$$\boldsymbol{z} = \begin{bmatrix} \frac{p_1}{p_3} f_1 \\ \frac{p_1}{p_3} f_2 \end{bmatrix} + \boldsymbol{v}, \tag{25}$$

where $\boldsymbol{z} \in \mathbb{R}^2$ are the 2D image coordinates, p_i denotes the ith translational component of $\mathcal{X}$, and f_i is the corresponding focal length. The measurement noise $\boldsymbol{v} \in \mathbb{R}^2$ is modeled with a standard deviation of 0.5 pixel in each direction. The 'naive' covariance matrix is set with a standard deviation of $7\,\text{cm}$ in the lateral directions of the end-effector and to $3\,\text{cm}$ for the longitudinal direction. The angular standard deviations are set to 5° and 15° respectively. In the order of magnitude, these values resemble the covariances from the PPOE model. The main difference is, that the PPOE covariance is configuration-dependent whereas this naive covariance is statically attached to the end-effector.

To validate our approach, we use the data from two experiments performed in our laboratory. We move the manipulator to different configurations, point the robot's cameras towards the arm and run the pose estimation. This setup is very similar to the LRU's configuration as shown in Fig. 1. In experiment I, the manipulator is moved to 9 configurations, where the end-effector is rotated significantly w.r.t. the camera. This requires the arm to be closer to the camera to allow for a detection of the small, inclined AprilTags of the end-effector. Experiment II considers the opposite scenario. In 29 configurations, the arm is stretched out - sometimes to the maximum reach - and the end-effector is barely rotated w.r.t. the camera. We grasp a VICON tracking target with the end-effector for ground truth measurements. Note that the LRU's end-effector is of rotational symmetrical peg-in-hole type. Once grasped, an object is precisely aligned in lateral direction, but residual errors remain in longitudinal direction and around the rotation axis. The evaluation metric is thus defined as the lateral distance between the estimated end-effector pose and the ground-truth obtained from the tracking target.

TABLE I: Mean error and standard deviation [cm] in the estimated position of the manipulator w.r.t. the ground truth.

Method	Covariance	Experiment I	Experiment II
forward kinematics	-	0.82 ± 0.49	1.48 ± 0.38
2D estimation	PPOE	0.29 ± 0.15	0.50 ± 0.25
2D estimation	naive	0.44 ± 0.29	0.52 ± 0.24

The results are displayed in Table I. The measured error of the forward kinematics is significantly smaller in experiment I than in II, illustrating the configuration dependency of the LRU's kinematic errors. The errors from experiment II, where the arm is stretched out further, are consistent in magnitude with the residual of the hand-eye calibration. This error magnitude underlines the need for pose correction algorithms.

Table I shows that for the experiment I, a significant estimation improvement is obtained when using the covari-

ance matrices computed with PPOE compared to the 'naive' approach. The covariance matrix of PPOE adapts to the significantly changed configuration of the robot, but the 'naive' covariance matrix remains constant. This causes a degradation in the accuracy of the estimation algorithms.

Contrary to this, the 2D pose correction of experiment II results in values that are largely similar regardless the type of covariance used. Experiment II ensured that the fiducial markers on the end-effector face towards the camera to ensure observability for all poses. This causes the 'naive' covariance matrix to locally coincide with the covariance matrix from PPOE for all configurations of II.

Summarized, it can be said that a static uncorrelated covariance matrix can represent the uncertainties of the forward kinematics in specific configurations, but fails to generalize for the complete workspace of the robot. Only a configuration-dependent error modeling like the PPOE model allows to consider forward kinematics as a consistent and reliable sensor for any configurations of the robot.

The fact that a residual error still exists for both cases indicates that systemic approaches to identify and quantify the error sources within kinematic chains are crucial for the use of the PPOE model, which will be part of future work.

VI. Conclusion

In this letter, we present the PPOE kinematics model – a novel approach for kinematic modeling of robots, which does not only consider the robot's deterministic geometry but also incorporates time and configuration dependent errors in a probabilistic way. We illustrate the PPOE model in an example and detail simplifications that are applied to it.

We specifically derive the PPOE model with a dedicated use in the field of sensor fusion in mind, focusing on sensor measurements that measure only a subset of the full end-effector pose. We provide two examples, where in both cases a significant improvement of the pose estimate is obtained using the PPOE model. The simulation showcases the benefits of correctly correlating the DoF of the error within the covariance matrix of the end-effector pose. In the experiment, we show that static covariances can provide valid measurements locally, but over the whole robot workspace, configuration dependency needs to be considered.

For future work, two principal aspects need to be mentioned. First, a systematic calibration approach needs to be developed that is capable of identifying the location and magnitude of error sources within the manipulator, thus allowing to precisely characterize the covariances of each error in the kinematics. Second, we plan to incorporate the PPOE model into dynamic pose estimation schemes that allow for online estimation of kinematic error parameters. Potential approaches consist of extending the EKF formulation of Section V-A by an online fusion scheme, alternatively applying particle filters to the system that include parameter identification approaches, or exploiting a factor graph based description of the system.

References

[1] M. J. Schuster, S. G. Brunner, K. Bussmann, S. Büttner, A. Dömel *et al.*, "Towards Autonomous Planetary Exploration: The Lightweight Rover Unit (LRU), its Success in the SpaceBotCamp Challenge, and Beyond," *Journal of Intelligent & Robotic Systems*, 2017.

[2] I.-M. Chen, G. Yang, C. T. Tan, and S. H. Yeo, "Local POE model for robot kinematic calibration," *Mechanism and Machine Theory*, vol. 36, no. 11, pp. 1215–1239, 2001.

[3] R. J. Webster and B. A. Jones, "Design and kinematic modeling of constant curvature continuum robots: A review," *The International Journal of Robotics Research*, vol. 29, no. 13, pp. 1661–1683, 2010.

[4] T. D. Barfoot and P. T. Furgale, "Associating uncertainty with three-dimensional poses for use in estimation problems," *IEEE Transactions on Robotics*, vol. 30, no. 3, pp. 679–693, 2014.

[5] S.-F. Su and C. S. G. Lee, "Manipulation and propagation of uncertainty and verification of applicability of actions in assembly tasks," *IEEE Transactions on Systems, Man, and Cybernetics*, vol. 22, no. 6, pp. 1376–1389, 1992.

[6] G. S. Chirikjian, *Stochastic Models, Information Theory, and Lie Groups, Volume 2*. New York: Birkhäuser Boston, 2011.

[7] Y. Wang and G. S. Chirikjian, "Nonparametric second-order theory of error propagation on motion groups," *The International Journal of Robotics Research*, vol. 27, no. 11-12, pp. 1258–1273, 2008.

[8] M. Brossard, S. Bonnabel, and A. Barrau, "Invariant Kalman filtering for visual inertial SLAM," in *International Conference on Information Fusion*, 2018, pp. 2021–2028.

[9] Y. Wang and G. S. Chirikjian, "Error propagation on the Euclidean group with applications to manipulator kinematics," *IEEE Transactions on Robotics*, vol. 22, no. 4, pp. 591–602, 2006.

[10] B. Siciliano and O. Khatib, Eds., *Springer Handbook of Robotics; 2nd Edition*. Berlin: Springer, 2016.

[11] R. Murray, *A Mathematical Introduction to Robotic Manipulation*. CRC Press, 1994.

[12] T. Schmidt, K. Hertkorn, R. Newcombe, Z. C. Marton, M. Suppa, and D. Fox, "Depth-based tracking with physical constraints for robot manipulation," in *IEEE International Conference on Robotics and Automation*, 2015, pp. 119–126.

[13] C. Garcia Cifuentes, J. Issac, M. Wüthrich, S. Schaal, and J. Bohg, "Probabilistic articulated real-time tracking for robot manipulation," *IEEE Robotics and Automation Letters*, vol. 2, pp. 577–584, 2017.

[14] T. E. Lee, J. Tremblay, T. To, J. Cheng, T. Mosier, O. Kroemer, D. Fox, and S. Birchfield, "Camera-to-robot pose estimation from a single image," in *IEEE International Conference on Robotics and Automation*, 2020, pp. 9426–9432.

[15] J. Solà, J. Deray, and D. Atchuthan, "A micro Lie theory for state estimation in robotics," Institut de Robòtica i Informàtica Industrial, Barcelona, Tech. Rep. IRI-TR-18-01, 2018.

[16] B. W. Mooring, Z. S. Roth, and M. R. Driels, *Fundamentals of manipulator calibration*. New York: Wiley, 1991.

[17] A. Long, K. Wolfe, M. Mashner, and G. Chirikjian, "The banana distribution is gaussian: A localization study with exponential coordinates," in *Robotics: Science and Systems*, 2012.

[18] G. Bourmaud, R. Mégret, A. Giremus, and Y. Berthoumieu, "Discrete extended kalman filter on lie groups," in *21st European Signal Processing Conference*, 2013, pp. 1–5.

[19] C. Hertzberg, R. Wagner, U. Frese, and L. Schröder, "Integrating generic sensor fusion algorithms with sound state representations through encapsulation of manifolds," *Information Fusion*, vol. 14, 2011.

[20] A. Raffin, B. Deutschmann, and F. Stulp, "Fault-tolerant six-DoF pose estimation for tendon-driven continuum mechanisms," *Frontiers in Robotics and AI*, vol. 8, 2021.

[21] M. Grebenstein, A. Albu-Schäffer, T. Bahls, M. Chalon, O. Eiberger, W. Friedl *et al.*, "The DLR Hand Arm System," in *IEEE International Conference on Robotics and Automation*, 2011.

[22] E. Olson, "Apriltag: A robust and flexible visual fiducial system," in *IEEE International Conference on Robotics and Automation*, 2011, pp. 3400–3407.

[23] K. H. Strobl and G. Hirzinger, "Optimal Hand-Eye Calibration," in *IEEE/RSJ International Conference on Intelligent Robots and Systems*, Beijing, China, 2006, pp. 4647–4653.